Real-time binary phase-only circular harmonic filters using a liquid crystal television in the Fourier plane of an optical correlator

Jean-Jacques P. Drolet*
Luc Leclerc†
Yunlong Sheng, MEMBER SPIE
Henri H. Arsenault, FELLOW SPIE
Université Laval
Centre d'Optique, Photonique et Laser
Québec, Canada G1K 7P4

Abstract. A rotation invariant optical correlator using a low-cost, liquid crystal television (LCTV) in the Fourier plane is described. The performance of the LCTV used as a filter support medium is evaluated, using interferometric measurements and an image reconstruction experiment. Different operating modes of an LCTV suitable for encoding binary phase-only filters are discussed. Finally, a modified LCTV is used in the filter plane of a conventional 4-f correlator to encode unipolar binary phase-only matched filters and unipolar binary phase-only circular harmonic filters. Optical experimental results are compared with the results of computer experiments.

Subject terms: information processing; liquid crystal television; binary phase-only filter; circular harmonic filter.

Optical Engineering 31(5), 939–946 (May 1992).

1 Introduction

Liquid crystal televisions (LCTVs) have been shown to provide a valuable substitute for costly spatial light modulators in a variety of optical data processing applications. Their properties have been extensively studied.[1–6] LCTVs have been used for simple image filtering,[7,8] computer-generated holography,[9,29] optoelectronic neural networks,[10] and image correlation in both conventional[1] and joint Fourier transform[11] correlators.

Although LCTVs are often used in optical correlators as the input device,[1,6–8,11,27] to the best of our knowledge, their use in the Fourier plane of an optical VanderLugt correlator has not been reported. One possible reason for this is the sensitivity of such a correlator to the optical quality of the filter support medium.[12] LCTVs are consumer display products, and optical quality is not a major concern in their design and manufacturing. For this reason, most LCTVs require modifications before being incorporated into optical signal processing systems. Other possible reasons for the absence of LCTVs in the optical filter plane is their relatively low contrast and low resolution, and also the fact that LCTV screens contain nonmodulating interpixel regions that introduce a dc peak in the impulse response of the filter and make the implementation of an on-axis binary phase-only filter (BPOF) difficult.[13]

Nevertheless, in a laboratory context, it is interesting to use a low-cost LCTV as a filter support medium in a real-time optical correlator. Moreover, the quality of the LCTVs on the market is rapidly improving in terms of contrast and resolution. Continuous phase-only modulation with an LCTV was recently reported.[14,15]

This paper presents a modified LCTV used to encode optical unipolar BPOFs in the Fourier plane of an optical correlator. Three important parameters for an LCTV used as a filter support are presented and discussed: modulation depth, random phase errors, and aspect ratio. As stated above, most LCTVs must be modified to improve their optical quality before they can be incorporated into an optical signal processor. The effectiveness of the modifications on our LCTV are evaluated. Different modes of operation of liquid crystal cells, corresponding to various types of BPOFs, are studied. Optical results for image reconstruction, correlation with binarized matched filters, and rotation invariant circular harmonic filtering are presented and compared with those obtained by computer experiments.

2 Liquid Crystal Televisions

2.1 *Principle of Operation*

Most liquid crystal televisions are based on a cell containing twisted nematic liquid crystals, as illustrated in Fig. 1. In their normal state, the liquid crystals are an anisotropic optical medium.[6,14] Their molecules can be modeled as tiny rods that tend to be roughly parallel to each other; their average orientation in a small neighborhood is called the *director*. During the fabrication process, a fine linear microstructure is designed on the inside faces of the glass plates enclosing the liquid crystal cell; the structures of the two plates are perpendicular to each other. The liquid crystal molecules that are near the plates tend to align themselves with those structures.[6] The liquid crystals therefore exhibit a helicoidal, or *twisted,* structure: the director undergoes a 90-deg rotation from one plate to the other. Under a simple condition (Mauguin's criterion)[14] that is met by all LCTVs

*Current affiliation: California Institute of Technology, Electrical Engineering Department, Pasadena, California 91125.
†Current affiliation: National Optics Institute, Sainte-Foy, Québec, Canada G1P 4N8.

Paper IP-005 received Aug. 7, 1991; revised manuscript received Dec. 12, 1991; accepted for publication Jan. 20, 1992.

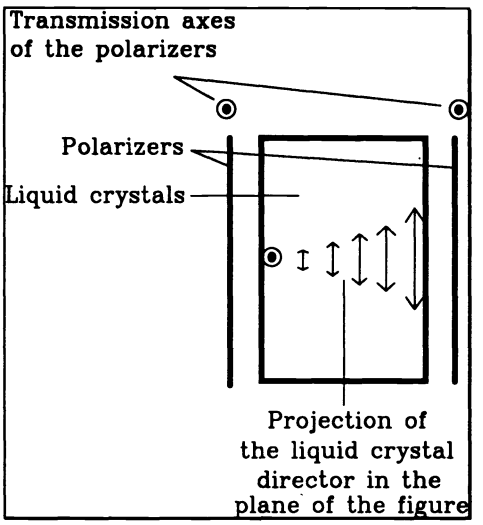

Fig. 1 A twisted nematic liquid crystal cell with two parallel polarizers.

under visible light illumination, a linearly polarized light beam that enters the cell with its polarization direction parallel to the director emerges as a linearly polarized beam, rotated by roughly 90 deg relative to the input beam. The liquid crystal director acts as a guide for the light polarization direction.

Therefore, when parallel polarizers are placed on both sides of the cell and are aligned with the liquid crystal director at the cell input, as illustrated in Fig. 1, the transmittance of the cell is very weak. The anisotropy that causes light rotation, however, is easily destroyed by the application of a small electric field. This is the purpose of the transparent electrodes present on both glass plates. When a voltage greater than a certain threshold is applied to the cell, most of the original anisotropy vanishes and the liquid crystals no longer significantly affect the light polarization. The cell thus becomes almost transparent. Therefore, the cell shown in Fig. 1, with its parallel polarizers, is an electrically addressable light amplitude modulator. An LCTV is a 2-D array of individually addressed liquid crystal cells, each of them similar to the arrangement of Fig. 1.

2.2 *Modulation Depth*

The liquid crystal television (LCTV) used in our experiments is a low-cost Realistic Pocketvision 5, model number 16-156, manufactured by Tandy Corporation. It counts 146×160 pixels, each of them measuring approximately 480 by 400 μm. The electric field applied to the liquid crystal cells is composed of two parts: a constant bias term, determined by a brightness control knob, and the video signal, which can be seen as an excursion from the bias that can be varied from pixel to pixel.

A commonly used measure of contrast for spatial light modulators is the *modulation depth,*[3] defined as

$$M = \frac{T_{\max} - T_{\min}}{T_{\max} + T_{\min}} , \tag{1}$$

where $T_{\min}$ and $T_{\max}$ are, respectively, the minimum and maximum transmissions of the modulator, corresponding to black and white pixels.

Ideally, one would like an SLM to have a maximum transmission near 100%, and a modulation depth equal to 1. On the Pocketvision 5, as on several other LCTVs, these requirements are somewhat contradictory: setting the brightness control for a high $T_{\max}$ yields a low contrast, and vice versa. There exists a brightness voltage that maximizes the contrast of the LCTV, but corresponds to a low $T_{\max}$. Under illumination by a collimated He-Ne beam ($\lambda = 632.8$ nm) having a diameter of 11 mm, with the brightness control adjusted for maximum contrast, the Pocketvision 5 was found to have a modulation depth of about 0.89. With $T_{\max} = 4\%$ and $T_{\min} = 0.23\%$, this translates into a contrast ratio ($T_{\max}/T_{\min}$) of 17:1.

The polarization angle modulation $\Delta\theta$ between the polarization axes of the emerging beams for light and dark pixels can be derived from the above transmission parameters, according the law of Malus:

$$\Delta\theta = \arccos\sqrt{T_{\min}} - \arccos\sqrt{T_{\max}} = 8.7 \text{ deg} . \tag{2}$$

Note, however, that this value is slightly inaccurate because the dead (i.e., nonmodulating) interpixel regions have not been taken into account. Moreover, the polarization rotation for white pixels is not constant, since the TV-rate raster scan causes an oscillation of the polarization rotation with a frequency equal to the scan rate. The value obtained above may therefore be considered as a time-averaged polarization angle modulation; the maximum instantaneous value of $\Delta\theta$ is larger. This oscillation is a hindrance to a good contrast. Fortunately, recent active matrix liquid crystal screens are much less subject to time variations of the polarization modulation, and can achieve higher time-averaged values for $\Delta\theta$.

2.3 *Scaling*

During early experiments, it was found that the Pocketvision 5 LCTV does not conform to the standard 4/3 aspect ratio common to most monitors. When the LCTV is controlled by a standard color graphics adapter, a square is displayed as a rectangle, and a circle as an ellipse. Of course, this would be a serious problem for matched filtering. Two correction methods for this problem come to mind: using a cylindrical lens system, or compensating the displayed images in software. The latter method was chosen. In addition to correcting the aspect ratio, it enables an image scaling that allows maximum use of the surface of the LCTV screen, thereby improving image quality. A computer program that performs two-dimensional scaling with independent scaling factors in the horizontal and vertical directions was written. It uses a simple linear interpolation algorithm. We found that horizontal and vertical expansion factors of 1.69 and 1.42, respectively, correct the aspect ratio problem, while maximizing the surface used on the LCTV screen.

2.4 *Phase Compensation*

The unmodified LCTV exhibits significant random phase errors over the surface of its screen. To improve its optical quality, the original glued sheet polarizers were first removed and replaced with good quality external dichroic polarizers, as suggested by Tai.[16] The optical flatness of the screen was then measured using a Zygo Mark III digital Fizeau interferometer. The optical path error over a circular area having a diameter of 5 cm was approximately three

He-Ne wavelengths. This corresponds to the optical quality of standard holographic plates.

The phase error may be compensated by immersing the screen in a liquid gate,[7–9] by gluing optical flats on the screen,[16] by using holographic phase-conjugate wavefront correction[28] and by coding a phase-correcting pattern into the images to be displayed.[17] We used the immersion technique with a mineral oil as the index matching fluid. The modified LCTV, immersed in the liquid gate, was tested with the Zygo interferometer. The flatness of the device over an area of approximately 6.7 cm^2 was decreased from 1λ without immersion to 0.3λ with immersion. In Sec. 4, we show that random phase errors on the LCTV screen introduce noise in reconstructed images, and that this noise is suppressed by immersing the LCTV in a liquid gate (see Fig. 4).

3 Unipolar BPOF Encoded by the LCTV

Liquid crystal televisions can operate in continuous intensity, phase, or polarization modulation modes.[4,14,15,18] In our case, we chose the binary phase-only modulation mode, with the LCTV controlled by a personal computer via a standard color graphics adapter (CGA).

Binary phase-only filters (BPOFs) provide sharp autocorrelation peaks and good discrimination capabilities.[13,19] They have been shown to be suitable for real-time optical data processing with a magneto-optic spatial light modulator.[20] Our goal is to encode a BPOF on a low-cost LCTV for pattern recognition.

Two different binary encodings of the phase of a filter $H(u,v)$ are commonly used. The most popular is the bipolar binary phase-only filter (BBPOF), obtained by simply thresholding the real or imaginary part of $H(u,v)$:

$$G_b(u,v)=\begin{cases}1 & \text{if } \mathrm{Re}[H(u,v)]>0\\ -1 & \text{otherwise}\end{cases} . \tag{3}$$

A slightly different encoding is for the unipolar binary phase-only filter[19] (UBPOF),

$$G_u(u,v)=\begin{cases}1 & \text{if } \mathrm{Re}[H(u,v)]>0\\ 0 & \text{otherwise}\end{cases} . \tag{4}$$

The unipolar BPOF, $G_u(u,v)$, is closely related to the bipolar BPOF, $G_b(u,v)$, by the simple relationship

$$G_u(u,v)=\frac{1}{2}[G_b(u,v)+1] , \tag{5}$$

so that it can also be considered as a BPOF. The BBPOF has a unit modulus, with phase values of $+\pi$ or $-\pi$. The UBPOF corresponds to a BBPOF plus a dc term.

Both bipolar and unipolar BPOFs are real, and their impulse responses must be Hermitian: $g(x,y)=g^*(-x,-y)$. Therefore, the binarization operation introduces a second object in the impulse response of the filter, which is rotated by 180 deg relative to the desired impulse response $h(x,y)$. This inverted ghost image is a major noise source in the BPOF. A simple method for avoiding this noise is to introduce a spatial carrier in $H(u,v)$ before the binarization.[13]

The UBPOF is easier to implement, since it requires only a simple on-off switching. Nevertheless, it contains a dc term that yields a bright central peak in its impulse response. The reconstructed objects must be shifted away from this peak by using a higher carrier frequency. This requires a higher space-bandwidth product for the SLM. The impulse response of an ideal BBPOF does not contain a central peak; therefore, a practical UBPOF requires a higher space-bandwidth product than the BBPOF. Moreover, the UBPOF has a lower energy efficiency than the BBPOF. Apart from those differences, the bipolar and unipolar BPOFs have similar properties for sharp autocorrelation peaks and good discrimination capability.[19]

Figure 2 illustrates how bipolar and unipolar BPOF modulations can be implemented on an ideal twisted nematic liquid crystal cell. Direction 1 is the polarization plane of the input beam. An output beam from a dark cell is rotated by 90 deg to direction 2, whereas light emerging from a white cell is aligned with direction 3.

A bipolar BPOF is obtained by aligning the output polarizer with direction 4 in Fig. 2(b), which is perpendicular to the median line between directions 2 and 3. The output beams from dark and light pixels, after passing through the analyzer, can take on values of -1 or $+1$. This method[20] can be used to encode a bipolar BPOF on a magneto-optic SLM. For the unipolar BPOF, the analyzer is aligned parallel to the polarization plane of the input beam, direction 1 in Fig. 2(a). This arrangement yields a {0,1} amplitude modulation.

The magneto-optic SLM is able to encode a bipolar BPOF, but as we will show, our LCTV is not able to encode this type of BPOF, because of the dc term of the LCTV. In fact, in our experiments, we always found a dc term in the LCTV whatever the orientation of the analyzer or the biasing conditions.

Assume that a filter $G(u,v,t)$ is displayed on the LCTV screen, where the time t is used as an explicit parameter in order to take into account the raster scanning of the video signal, the intensity of the center of the impulse response is

$$I(0,0)\propto \int_{\tau}^{\tau+T}\left|\int_{-\infty}^{\infty}\int_{-\infty}^{\infty} G(u,v,t)\,du\,dv\right|^2 dt , \tag{6}$$

where T is the raster scan period and τ is an arbitrary time. From Eq. (6), a necessary condition for the absence of a dc peak [i.e., $I(0,0)=0$] is that the instantaneous space-averaged screen transmittance,

$$\int_{-\infty}^{\infty}\int_{-\infty}^{\infty} G(u,v,t)\,du\,dv , \tag{7}$$

always be equal to zero. Two factors contribute to the dc peak by preventing the above integral to be null at all times: the dead interpixel regions and the time variation of the polarization angle modulation.

The dead interpixel regions are a 2-D grid covered by the conductor lines on the LCTV where the liquid crystal material is almost unaffected by the electrical signal. This contributes an additional term to the required filter $G(u,v)$ and leads the spatial integral of Eq. (7) to be nonzero.

The pixels on the LCTV screen are updated asynchronously by a raster scan mechanism using electrode time mul-

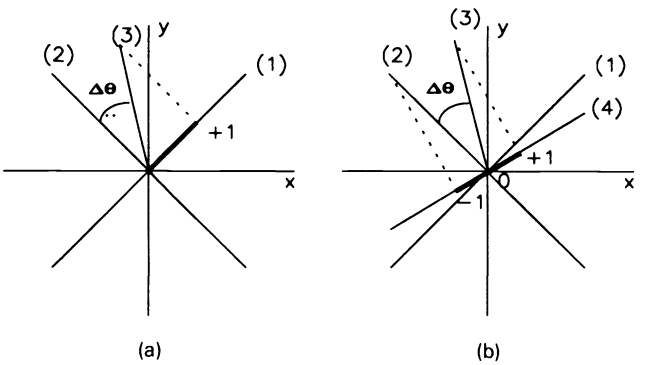

Fig. 2 Implementation of a unipolar (a) and bipolar (b) binary phase-only filter on an ideal twisted nematic liquid crystal modulator. Directions 1, 2, and 3 are, respectively, the transmission axis of the input polarizer, the polarization direction of output light for a dark pixel, and the polarization direction of output light for a white (transparent) pixel. For the UBPOF, the input and output polarizers are parallel, and the output can assume normalized values of 0 or +1. For the BBPOF, the output polarizer is aligned[16,22] with direction 4, and the output can take on normalized values of −1 or +1.

tiplexing. The anisotropy of white pixels is not constant, but decays during a raster scan cycle. Different pixels are on different points of the decay curve, depending on their position on the screen. Since the natural symmetry of the filter is hindered by the raster scan mechanism and by the finite relaxation time of the liquid crystal material, it is very unlikely that the integral of Eq. (7) will be null at all times.

Because of the dc term on the LCTV, the light efficiency of the filter decreases. An attempt to encode an on-axis BPOF would result in a severe degradation of the impulse response caused by the dc term noise. The impulse response must then be isolated from the dc peak by using a higher carrier frequency, just as with the unipolar BPOF. Thus, the advantages of the bipolar BPOF over the unipolar BPOF vanish.

In practice, an LCTV can neither completely extinguish the input beam nor have a total transmittance. Therefore, the amplitude modulation performed by the LCTV is $\{C,D\}$ rather than $\{0,1\}$. The values of C and D depend on the biasing and addressing conditions of the LCTV. From Sec. 2.2, we obtain the values $C=(0.0023)^{1/2}=0.048$ and $D=(0.04)^{1/2}=0.20$. The filter $\{C,D\}$ is equivalent to a unipolar BPOF $\{0,1\}$ multiplied by $D-C$, plus C.

In the above configuration, the LCTV performs a polarization modulation, which is translated into an amplitude modulation by the analyzer. In our experiments, we found that the LCTV can operate even without using an analyzer. This phenomenon was first observed and explained by Tam.[14] In fact, the LCTV yields a 2-D image just after its screen, in which all the pixels have the same amplitude, but two different polarization orientations. The far-field diffraction of this polarization modulated image can be seen as a superposition of two diffraction patterns. One has its polarization axis parallel to direction 2 in Fig. 2(a), with an amplitude modulation of $\{1, \cos \Delta\theta\}$, whereas the other has its polarization axis perpendicular to direction 2, with an amplitude modulation of $\{0, \sin \Delta\theta\}$, where $\Delta\theta$ is the angle between directions 2 and 3, i.e., the angle of polarization modulation. Since the two patterns have perpendicular polarizations, they do not interfere with each other. The image detected by a square-law detector in the far field is the sum of the intensities of those two diffraction patterns. The LCTV can therefore operate without an analyzer. In this operation mode, we have two similar unipolar BPOFs with different amplitude modulations. Their outputs are superimposed by addition of intensity. This mode increases the light efficiency of the desired impulse response. However, the dc peak is also increased because the filter $\{1, \cos \Delta\theta\}$ contains a significant dc term.

4 Image Reconstruction

A simple image reconstruction experiment was performed to confirm the LCTVs ability to be used as a filter support medium. The unipolar BPOF $G_u(u,v)$ of an object $h(x,y)$ was computed according to Eq. (4) and fed to the LCTV by a computer via the video input jack. The inverse Fourier transform $g(x,y)$ of $G_u(u,v)$ is a reconstruction of the object $h(x,y)$, which mainly consists of its edges because of the high-pass property of the BPOF. The pixel grid structure of the LCTV screen forms a well-developed regular diffraction pattern in the output plane. The LCTV features a regular pixel grid, where each pixel has width and height of a and b, respectively, and where the horizontal and vertical center-to-center distances between two pixels are, respectively, α and β, as shown in Fig. 3. On the Pocketvision 5, we have $\alpha=482$ μm and $\beta=406$ μm. Remember from Sec. 3 that the LCTV translates a UBPOF $G(u,v)$ having values of $\{0,1\}$ into transmittances of $\{C,D\}$, where $C\neq 0$. The transmittance of the screen displaying the filter $G(u,v)$ is given by

$$D(u,v)=\sum_m\sum_n \operatorname{rect}\left[\frac{u\lambda f-m\alpha}{a}, \frac{v\lambda f-n\beta}{b}\right] \times\left[(D-C)G\left(\frac{m\alpha}{\lambda f}, \frac{n\beta}{\lambda f}\right)+C\right], \tag{8}$$

where f is the focal length of the Fourier transform lens. In our experiments, $f=180$ cm. The LCTV is illuminated with a collimated He-Ne beam with $\lambda=632.8$ nm. Taking the inverse Fourier transform, it can be shown[21] that the reconstruction plane is given by

$$d(x,y)\cong\frac{ab}{\lambda^2 f^2}\sum_m\sum_n\left\{\operatorname{sinc}\left(\frac{am}{\alpha}\right)\operatorname{sinc}\left(\frac{bn}{\beta}\right) \times\left[(D-C)g\left(x-\frac{m\lambda f}{\alpha}, y-\frac{n\lambda f}{\beta}\right) +C\delta\left(x-\frac{m\lambda f}{\alpha}, y-\frac{n\lambda f}{\beta}\right)\right]\right\}. \tag{9}$$

Each pair of values (m,n) can be seen as designating a diffraction order in the reconstruction plane. Each such order contains a Dirac delta function and a reconstructed image $g(x,y)$. The reconstruction of a BPOF, $g(x,y)$, contains two objects: the desired object and a ghost inverted image. When a spatial frequency carrier is used, these objects are shifted symmetrically relative to the central delta function. The relative intensities of the different diffraction orders are

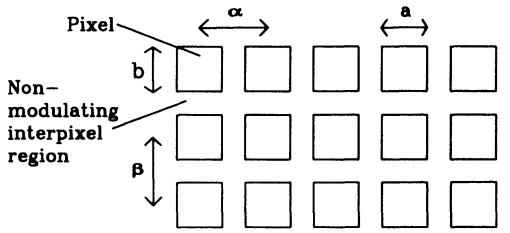

Fig. 3 Model of the LCTV screen.

governed by the two sinc functions. The horizontal and vertical distances between diffraction orders, respectively given by $\lambda f/\alpha = 2.4$ mm and $\lambda f/\beta = 2.8$ mm, agree with those measured on experimental reconstructions such as those of Fig. 4.

Reconstructions of the outline of a space shuttle are shown in Fig. 4(a) with and in Fig. 4(b) without immersion of the LCTV screen in the liquid gate. The immersion obviously reduces the noise in the reconstructed image caused by random phase errors in the LCTV glass plates. The double reconstruction is a natural consequence of binarizing the matched filter; the diffraction orders are attributable to the pixel grid of the LCTV and to the dead interpixel areas, as discussed above.

Since the obtained reconstructions are very sharp and clear, our modified LCTV is ready to be used in the filter plane of a 4-f optical correlator.

5 Correlation with a BPOF

A conventional 4-f image correlator using a LCTV in its filter plane is illustrated in Fig. 5. The alignment of the filter plane of such a correlator is often critical. With the use of a computer-controlled LCTV in its filter plane, its alignment can be greatly simplified if the computer can shift the displayed filter on the LCTV screen in tiny increments. A custom software program was written for this purpose. It also provides an arbitrary scaling capability that is useful in matching the size of the filter to the optically generated Fourier transform of the input scene.

The results of two optical correlation experiments are presented in Figs. 6 and 7. The former used binary letters of the roman alphabet, whereas the latter used the binarized images of several aircraft. The filters displayed on the LCTV were unipolar BPOFs obtained from the Fourier transforms of the reference objects multiplied by an appropriate carrier in order to shift the correlation function away from the zero-order diffraction pattern in the output plane. In the first experiment, the reference image is the letter E; the maximum intensity of its correlation with each of the letters E, F, P, M, G, I, and A is illustrated in Fig. 6. The experimental results are presented alongside the correlation intensities predicted by a computer simulation of a hypothetical correlator featuring ideal spatial light modulators (modulation depth equal to one, no dead regions) in its input and filter planes.

Although the discrimination capability of the LCTV correlator is not exactly as good as predicted by the computer simulation, experimental and simulated correlation peak intensities definitely follow similar trends, and there are no false alarms. The correlation intensity corresponding to the worst discrimination case (letter F) is only 47% of the autocorrelation of the letter E, which is a very good performance.

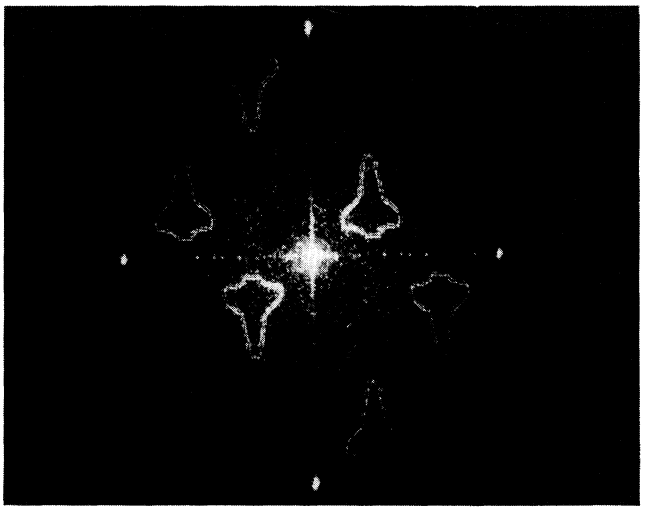

(a)

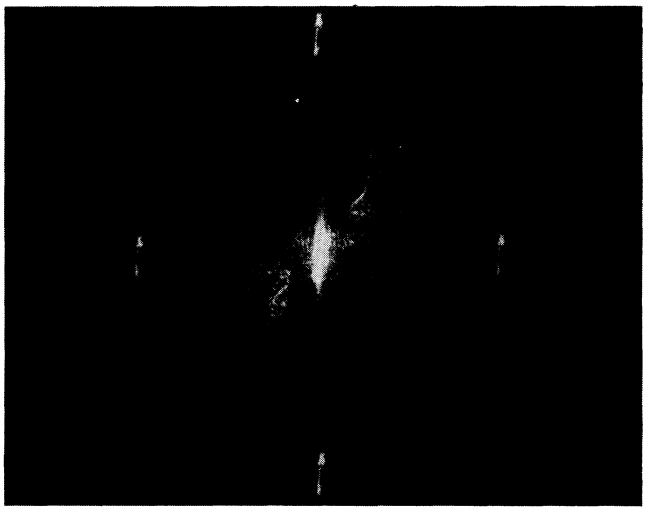

(b)

Fig. 4 Reconstruction of the outline of a space shuttle from its binary phase-only matched filter displayed on the LCTV, with (a) and without (b) immersion in a liquid gate.

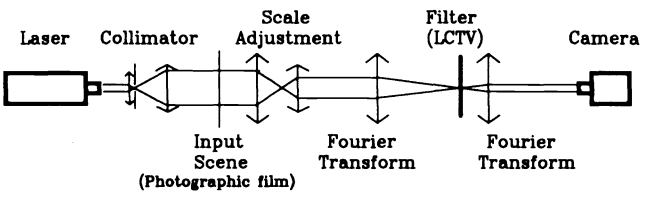

Fig. 5 The LCTV is used as the support medium for binary phase-only filters in the Fourier plane of a conventional 4-f image correlator.

An American space shuttle is used as the reference image for the second experiment. The peak intensities of its correlation with several aircraft (shuttle with bay open, Lightning, SST, X-29, F-102A and glider, illustrated in Fig. 8) were calculated on a computer and compared to the outputs

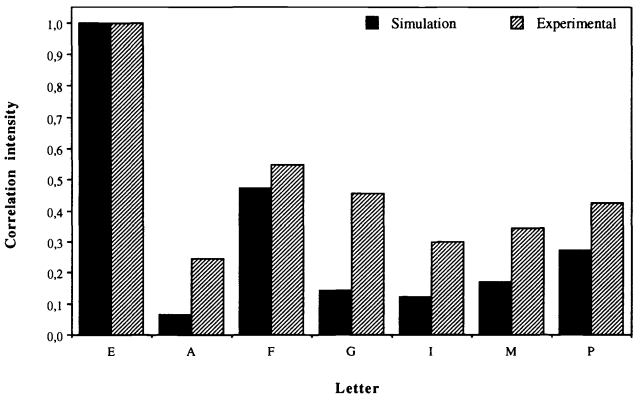

Fig. 6 Correlation peak intensities of seven letters of the roman alphabet with the binary phase-only filter of letter E.

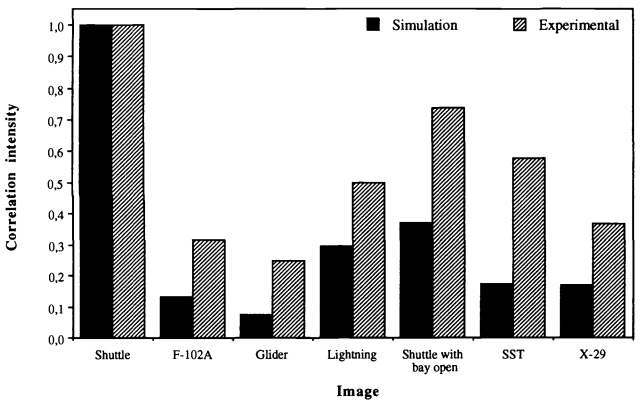

Fig. 7 Correlation peak intensities. The LCTV displays the binary phase-only filter of the shuttle.

measured on the optical correlator. The results are presented in Fig. 7.

Here again, the correlator functions as expected. The worst performance is with the shuttle with bay open, whose detection level is 74% of that obtained for the shuttle with bay shut. The discrimination capability is still good, although not as much as that obtained with the letters.

6 Circular Harmonic Filtering

Any image $f(r,\theta)$ can be expressed as a circular harmonic expansion

$$f(r,\theta)=\sum_{m=-\infty}^{\infty} f_m(r)\,\exp(jm\theta)\ , \tag{10}$$

where

$$f_m(r)=\frac{1}{2\pi}\int_0^{2\pi} f(r,\theta)\,\exp(-jm\theta)\,d\theta\ . \tag{11}$$

The m'th term in the above series is called the m'th circular harmonic component of the object $f(r,\theta)$. It can be shown[22] that the intensity of the correlation of an object with any of its circular harmonic components is rotation and translation

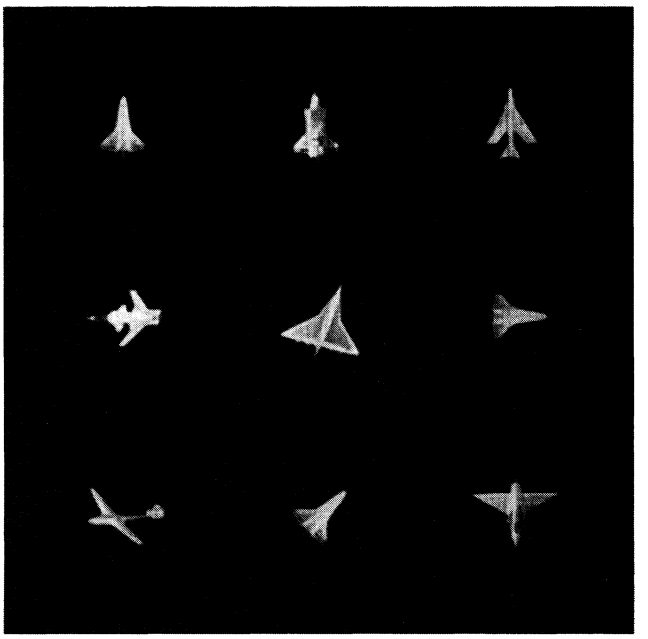

Fig. 8 Images of aircraft whose correlation with the space shuttle was performed by the optical correlator. From left to right and top to bottom: upright shuttle, shuttle with bay open, Lightning, X-29, SST, shuttle rotated by 90 deg, glider, shuttle rotated by 45 deg, and F-102A.

invariant. One can therefore provide a correlator with rotation invariance by substituting the Fourier transform of a circular harmonic component of the reference object for the matched filter. This Fourier transform is called a circular harmonic filter.

A binary phase-only circular harmonic filter (BPOCHF) can be obtained from a circular harmonic filter exactly as a BPOF is obtained from a matched filter. The resulting filter is rotation invariant and has a good discrimination capability.[19,23,24]

Two series of rotation invariant correlation results are presented, one for letters of the roman alphabet, and one for aircraft. The filter displayed on the liquid crystal television was the second-order BPOCHF of the reference object.

Figure 9 illustrates the correlation peak intensities for the letters A, upright E (E,000), E rotated by 45 deg (E,045), E rotated by 90 deg (E,090), F, G, I, M and P. As before, the reference image is the upright letter E. Since the correlation intensities of the three rotated reference images are almost equal, rotation invariance is achieved. A comparison of Figs. 6 and 9 makes it obvious that the addition of rotation invariance somewhat decreases the discrimination capabilities of the correlator. Nevertheless, there are no false alarms, and the performance of the LCTV correlator is still good. The relatively low correlation peak produced by the computer-simulated correlator for letter E rotated by 45 deg is attributable to aliasing.

Correlation results for the set of aircraft images are presented in Fig. 10. Here again, rotation invariance is obtained. The F-102A airplane, however, is detected almost as strongly as the shuttles. Several other airplanes have detection levels that are very close to that of the shuttles. This could make the correlator unreliable in the presence of noise. Therefore, our rotation invariant correlator seems

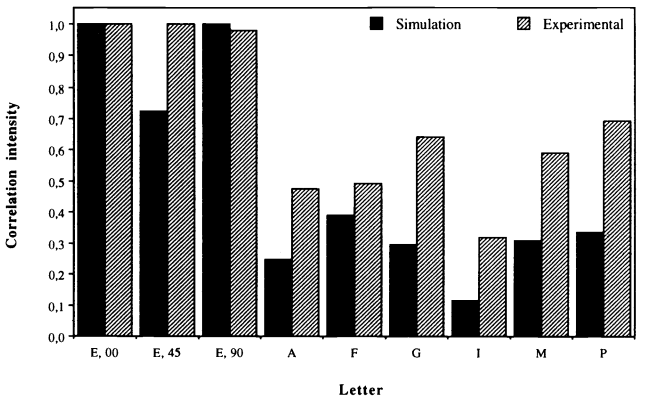

Fig. 9 Correlation peak intensities for letters of the roman alphabet. The LCTV displays the binary phase-only second-order circular harmonic filter of the letter E.

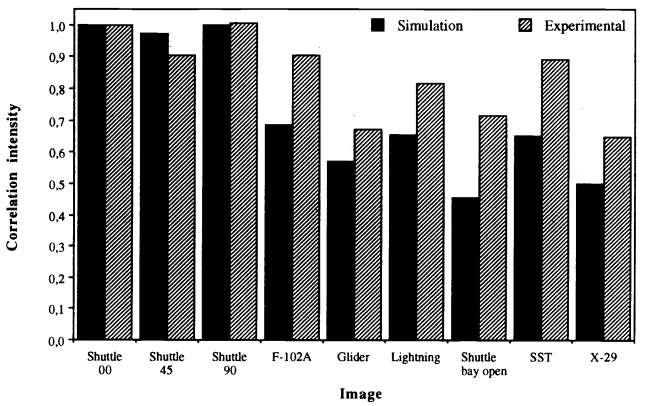

Fig. 10 Correlation peak intensities. The LCTV displays the binary phase-only second-order circular harmonic filter of the upright shuttle.

to be more reliable with letters than with aircraft. For the latter, discrimination could be increased by using circular harmonic composite filters or other discrimination-enhancing methods.[25,26]

7 Conclusion

A low-cost modified LCTV has been used in the Fourier plane of a real-time VanderLugt optical correlator. Because of the low contrast and low resolution of the LCTV, and due to the inevitable presence of a dc peak in the impulse response of a filter displayed on the device, the LCTV is most suitable to display unipolar BPOFs. Coupled with adequate computer software, the LCTV eases the alignment of the correlator. Experimental results for optical binarized matched filters and rotation invariant circular harmonic filters using the LCTV show good performance, comparable to that obtained by computer simulation of an ideal modulator. An optical correlator with an LCTV in its filter plane can be used for laboratory experimentation when a costly magneto-optic SLM is not available. LCTVs have a definite potential to be used in the filter plane of real-time optical correlators, especially with their rapidly improving contrast and resolution.

Acknowledgments

We express our gratitude to Lin Li for his help during the interferometric measurements. This research was supported in part by the Natural Sciences and Engineering Research Council of Canada and the Fonds pour la Formation des Chercheurs et l'Aide à la Recherche du Québec.

References

1. H. K. Liu, J. A. Davis, and R. A. Lilly, "Optical-data-processing properties of a liquid-crystal television spatial light modulator," *Opt. Lett.* **10**(12), 635–637 (1985).
2. J. A. McEwan, A. D. Fisher, P. B. Rolsma, and J. N. Lee, "Optical-processing characteristics of a low-cost liquid crystal display device," *J. Opt. Soc. Am.* **2**(13), 8 (1985).
3. G. D. Boreman and E. R. Raudenbush, "Modulation depth characteristics of a liquid crystal television spatial light modulator," *Appl. Opt.* **27**(14), 2940–2943 (1988).
4. E. Kaneko, "Liquid crystal TV displays: Principles and applications of liquid crystal displays," in *Advances in Optoelectronics,* T. Okoshi, Ed., KTK Scientific Publishers (1988).
5. K. Lu and B. E. A. Saleh, "Theory and design of the liquid crystal TV as an optical spatial phase modulator," *Opt. Eng.* **29**(3), 240–246 (1990).
6. H. K. Liu and T. H. Chao, "Liquid crystal television spatial light modulators," *Appl. Opt.* **28**(22), 4772–4780 (1989).
7. M. Young, "Low-cost LCD video display for optical processing," *Appl. Opt.* **25**(7), 1024–1026 (1986).
8. F. T. S. Yu, S. Jutamulia, and X. L. Huang, "Experimental application of low-cost liquid crystal TV to white-light optical signal processing," *Appl. Opt.* **25**(19), 3324–3326 (1986).
9. F. Mok, J. Diep, H. K. Liu, and D. Psaltis, "Real-time computer-generated hologram by means of liquid-crystal television spatial light modulator," *Opt. Lett.* **11**(11), 748–750 (1986).
10. F. T. S. Yu, T. Lu, and X. Yang, "Optical neural network with pocket-sized liquid-crystal televisions," *Opt. Lett.* **15**(15), 863–865 (1990).
11. F. T. S. Yu, S. Jutamulia, T. W. Lin, and D. A. Gregory, "Adaptive real-time pattern recognition using a liquid crystal TV-based joint transform correlator," *Appl. Opt.* **26**, 1370–1372 (1987).
12. J. L. Horner, "Is phase correction required in SLM-based optical correlators?" *Appl. Opt.* **27**(3), 436–438 (1988).
13. J. L. Horner and J. Leger, "Pattern recognition with binary phase-only filters," *Appl. Opt.* **24**, 609–611 (1985).
14. E. Tam, PhD Thesis, "Modulation properties of a twisted nematic liquid crystal spatial light modulator and its application in a joint transform correlator," Pennsylvania State University (1990).
15. J. C. Kirsch, J. A. Laudin, and D. A. Gregory, "Hybrid modulation properties of the Epson LCTV," Proc. SPIE **1558**, 432–441 (1991).
16. A. M. Tai, "Low-cost LCD spatial light modulator with high optical quality," *Appl. Opt.* **25**(9), 1380–1382 (1986).
17. H. M. Kim, J. W. Jeong, M. H. Kang, and S. I. Jeong, "Phase correction of a spatial light modulator displaying a binary phase-only filter," *Appl. Opt.* **27**(20), 4167–4168 (1988).
18. N. Konforti, E. Marom, and S. T. Wu, "Phase-only modulation with twisted nematic liquid-crystal spatial light modulators," *Opt. Lett.* **13**(3), 251–253 (1988).
19. L. Leclerc, Y. Sheng, and H. H. Arsenault, "Optical binary phase-only filters for circular harmonic correlations," *Appl. Opt.* **30,** 4643–4649 (1991).
20. D. Psaltis, E. G. Paek, and S. S. Venkatesh, "Optical image correlation with a binary spatial light modulator," *Opt. Eng.* **23**(6), 698–704 (1984).
21. L. Leclerc, "Etude comparative de différentes méthodes de filtrage de phase d'harmoniques circulaires," PhD Thesis, Université Laval (1992).
22. Y. N. Hsu, H. H. Arsenault, and G. April, "Rotation-invariant digital pattern recognition using the circular harmonic expansion," *Appl. Opt.* **21**, 4012–4015 (1982).
23. J. Rosen and J. Shamir, "Circular harmonic phase filters for efficient rotation-invariant pattern recognition," *Appl. Opt.* **27**, 2895–2899 (1988).
24. L. Leclerc, Y. Sheng, and H. H. Arsenault, "Rotation invariant phase-only and binary phase-only correlation," *Appl. Opt.* **28**(6), 1251–1256 (1989).
25. Y. Sheng, L. Leclerc, and H. H. Arsenault, "Multiplexed binary phase-only circular harmonic filters," Proc. SPIE **1564**, 320–329 (1991).
26. L. Leclerc, Y. Sheng, and H. H. Arsenault, "Circular harmonic covariance filters for rotation invariant object recognition and discrimination," *Opt. Comm.* **85,** 299–305 (1991).

27. D. Gregory, "Real-time pattern recognition using a modified liquid crystal television in a coherent optical correlator," *Appl. Opt.* **25**, 467–469 (1986).
28. D. Casasent and S. F. Xia, "Phase correction of light modulators," *Opt. Lett.* **11**, 398–400 (1986).
29. N. Hashimoto, S. Morokawa, and K. Kitamura, "Real-time holography using the high-resolution LCTV-SLM," in *Practical Holography V,* Proc. SPIE **1461**, 291–302 (1991).

Jean-Jacques P. Drolet received the BSc degree in engineering physics from Université Laval, Québec, in 1990. He was a recipient of the NSERC 1967 Scholarship and of the John H. Chapman Award from Spar Aerospace. In 1990 and 1991, he was a defence scientist with the Canadian Department of National Defence and a research assistant with the National Optics Institute of Canada. He is now pursuing graduate studies in the Department of Electrical Engineering at the California Institute of Technology. His research interests include optical information processing, pattern recognition, and neural networks.

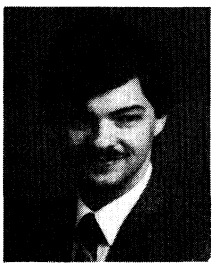

Luc Leclerc is a researcher at the National Optics Institute, Québec, Canada. He received the BSc degree in engineering physics in 1986 and the MSc degree in physics (optics) in 1987 from Université Laval, Québec, Canada. Since then, he has pursued graduate studies in optics in the Centre d'Optique, Photonique et Laser at Université Laval, where he has just completed his PhD. His research interests are optical pattern recognition, image processing, holography, and diffractive elements.

Yunlong Sheng received his BS degree in jet propulsion thermophysics from the University of Science and Technology of China, Beijing, in 1964. He received his MS, doctor and docteur d'état degrees in physics from Université de Franche-Comté, Besançon, France, in 1980, 1982 and 1986, respectively. Since 1985, he has been a research associate and assistant professor at Université Laval. Dr. Sheng is a member of OSA and SPIE. His research interests involve optical image processing, invariant pattern recognition, and optical computing. He is author and co-author of 50 publications, including two chapters of books and the book *Optical Computing.*

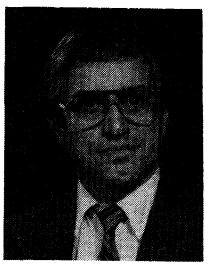

Henri H. Arsenault is a professor in the Department of Physics at Université Laval, in Québec City, Canada. He is the author of more than 70 publications in optical and digital information processing, pattern recognition, optical computing, and artificial intelligence. He is a fellow of the Optical Society of America and of SPIE. He has filled a number of functions in optical societies. He is co-editor of the book *Optical Processing and Computing,* co-author of the book *Optical Computing,* and has contributed chapters to various books, the most recent being a chapter on optical computers for the *Computer Engineering Handbook.*